Advances in Materials Research, *Vol. 11*, *No. 1* (*2022*) *41-57*
https://doi.org/10.12989/amr.2022.11.1.041

Analysis of the strain energy release rate for time-dependent delamination in multilayered beams with creep

Victor I. Rizov*

Department of Technical Mechanics, *University of Architecture*,
Civil Engineering and Geodesy, *1 Chr. Smirnensky blvd.*, *1046 - Sofia*, *Bulgaria*

(*Received April 5*, *2021*, *Revised September 30*, *2021*, *Accepted January 18*, *2021*)

Abstract. This paper is focused on delamination analysis of a multilayered inhomogeneous viscoelastic beam subjected to linear creep under constant applied stress. The viscoelastic model that is used to treat the creep consists of consecutively connected units. Each unit consists of one spring and two dashpots. The number of units in the model is arbitrary. The modulus of elasticity of the spring in each unit changes with time. Besides, the modulii of elasticity and the coefficients of viscosity change continuously along the thickness, width and length in each layer since the material is continuously inhomogeneous in each layer of the beam. A time-dependent solution to the strain energy release rate for the delamination is derived. A time-dependent solution to the *J*-integral is derived too. A parametric analysis of the strain energy release rate is carried-out by applying the solution derived. The influence of various factors such as creep, material inhomogeneity, the change of the modulii of elasticity with time and the number of units in the viscoelastic model on the strain energy release rate are clarified.

Keywords: analytical study; creep; delamination; inhomogeneous material; multilayered beam

1. Introduction

Multilayered load-bearing beam structures consist of adhesively bonded longitudinal layers of different materials. Multilayered materials and structures are attracting considerable attention mainly because of increasing demands for high performances in various structural applications in modern engineering (Abderezak *et al*. 2021, Rabia *et al*. 2020). Also, by using multilayered materials, one can achieve significant reduction of structural weight since multilayered materials have high strength to weight and stiffness to weight ratios. Therefore, multilayered materials are widely used in aeronautics, civil engineering, car industry and other engineering applications where structural weight is an important issue.

Although multilayered materials and structures are quite modern, they have some substantial drawbacks. For example, multilayered structural members are rather vulnerable to delamination fracture due to their low interlayer strength. Delamination (i.e., separation of layers) affects the integrity and reliability of multilayered structures and reduces their strength and stiffness. In fact, delamination is the most common failure mechanism in multilayered load-bearing structures. The principles of fracture mechanics have been frequently applied to analyze the delamination in

*Corresponding author, Professor, E-mail: V_RIZOV_FHE@UACG.BG

http://www.techno-press.org/?journal=amr&subpage=5 ISSN: 2234-0912 (Print), 2234-179X (Online)

multilayered materials. One of the basic purposes of the delamination analyses is to derive solutions to the strain energy release rate (Hsueh *et al*. 2009, Malzbender 2004, Hutchinson and Suo 1991).

Delamination fracture of linear-elastic multilayered beam structures is performed by Hsueh *et al*. (2009). The beams under consideration are simply supported. They are loaded in four-point bending symmetrically with respect to the mid-span. A central notch is cut under the top surface of the beam in order to induce conditions for delamination fracture. Closed-form solution of the strain energy release rate is found for delamination crack located in the central portion of the beam (between the two external forces).

Analytical studies of delamination in multilayered structural materials are developed in (Malzbender 2004). The delamination is caused by external bending moments and thermal loading. Delamination in functionally graded elastic materials is also analyzed. A methodology for deriving of the strain energy release rate for delamination crack in multilayered materials is presented (Malzbender 2004).

Delamination analyses of layered beam structures with linear-elastic behavior are reviewed and discussed in (Hutchinson and Suo 1991). Various analytical solutions of the strain energy release rate for delamination cracks derived by applying the methods of linearly-elastic fracture mechanics are presented. Delaminted beam configurations subjected to different loading conditions are considered (Hutchinson and Suo 1991).

It should be mentioned that the delamination fracture is a topical problem also for continuously inhomogeneous structural materials. This is due to the fact that such continuously inhomogeneous materials as functionally graded ones can be built-up layer by layer (Mahamood and Akinlabi 2017, Miyamoto *et al*. 1999) which is a premise for appearance of delamination cracks. The material properties of continuously inhomogeneous materials depend on the coordinates (Ahmed *et al*. 2020, Kurşun *et al*. 2012, 2014, Kurşun and Topçu 2013, Arda 2020, Arda and Aydogdu 2016, Butcher *et al*. 1999, Gasik 2010, Hedia *et al*. 2014, Aydogdu *et al*. 2018). Since the variation of the properties of continuously inhomogeneous (functionally graded) materials in the solid can be formed technologically, these materials are now widely employed in various areas of practical engineering (Uymaz 2013, 2014a, b, Mahamood and Akinlabi 2017, Markworth *et al*. 1995, Miyamoto *et al*. 1999, Nemat-Allal *et al*. 2011, Wu *et al*. 2014).

In contrast to previous papers which deal with instantaneous delamination in multilayered beams (Hsueh *et al*. 2009, Malzbender 2004, Hutchinson and Suo 1991, Rizov 2016, 2017, 2018, 2020, Rizov and Altenbach 2019, Rizov and Altenbach 2020a, b) or with longitudinal fracture of inhomogeneous viscoelastic beams (Rizov 2021), the present paper is concerned with analysis of time-dependent delamination in a multilayered inhomogeneous beam configuration that exhibits linear creep behavior. The paper is motivated also by the fact that viscoelastic materials are used frequently in layered structures (Nguyen *et al*. 2015, 2020). Therefore, analyzing of delamination in layered beams under creep is an important problem for practical engineering. It should be noted that the present paper studies also the effect of change of the modulus of elasticity with time on the delamination under creep since this effect is not clarified in previous studies (Rizov 2020). A viscoelastic model with arbitrary number of consecutively connected units is used for describing of creep in the present paper. Each unit of the model has one spring whose modulus of elasticity changes with time and two dashpots. The beam layers are inhomogeneous along their width, thickness and length. Therefore, the modulus of elasticity and the coefficients of viscosity vary continuously in each layer. A time-dependent solution to the strain energy release rate that accounts for the creep is derived. The solution can be applied for a delamination crack located

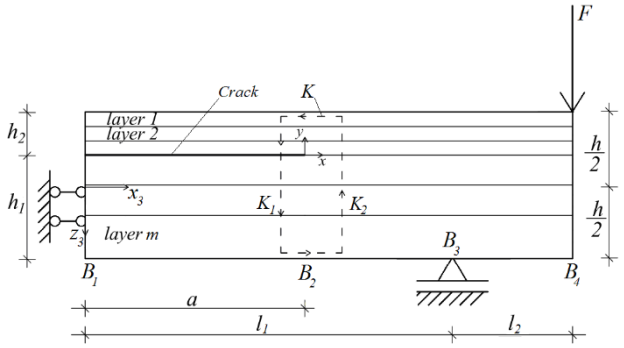

Fig. 1 Geometry and loading of a multilayered beam with a delamination crack

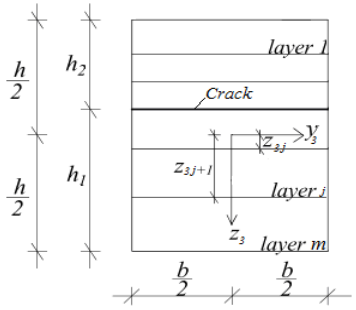

Fig. 2 Cross-section of the beam

arbitrary between layers. The *J*-integral approach is used for verification of the time-dependent solution to the strain energy release rate.

2. Theoretical model of delaminated multilayered inhomogeneous beam with creep

The present paper deals with the multilayered inhomogeneous viscoelastic beam configuration depicted in Fig. 1. The beam is made of adhesively bonded inhomogeneous layers with individual properties and thicknesses. The cross-section of the beam is a rectangle of width, b, and thickness, h, as shown in Fig. 2. The length of the beam is $l_1 + l_2$. A delamination crack of length, a, is located between layers. The thicknesses of the lower and upper delamination crack arms are h_1 and h_2, respectively (Fig. 1). A roller in point, B_3, and a Q-apparatus in the free end of the lower delamination crack arm are used to support the beam. The external loading consists of a vertical force, F, applied at right-hand end of the beam (Fig. 1). The crack is located in beam portion, B_1B_3, that is loaded in pure bending. It is obvious that the upper delamination crack arm is free of stresses.

Each layer of the beam exhibits creep behavior that is treated by using the linear viscoelastic model shown in Fig. 3. The model consists of n consecutively connected units. Each unit consists of one spring with modulus of elasticity, E_{ij}, and two dashpots with coefficients of viscosity, $\eta_{D_{ij}}$ and $\eta_{H_{ij}}$, where subscripts i and j refer to the unit of the viscoelastic model and to layer of the beam, respectively.

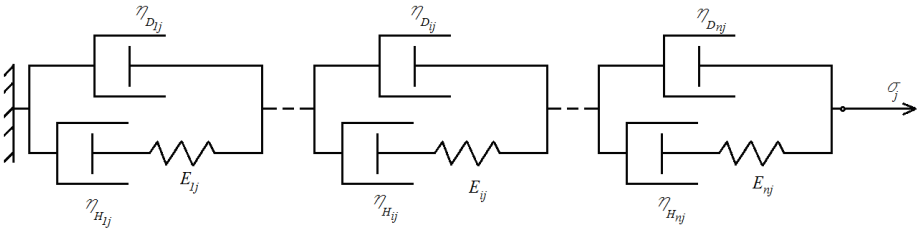

Fig. 3 Viscoelastic model

The modulus of elasticity in the *i*-the unit of the model for the *j*-th layer of the beam changes smoothly with time, t, according to the following hyperbolic law

$$E_{ij} = E_{0_{ij}}\left[1 + f_{ij}\left(1 - \frac{1}{1+t}\right)\right] \tag{1}$$

where

$$i = 1,2,\ldots n \tag{2}$$

$$j = 1,2,\ldots m \tag{3}$$

In the above formulae, m is the number of layers in the beam, $E_{0_{ij}}$ is the initial value of the modulus of elasticity, f_{ij} is a material property that controls the change of the modulus of elasticity with time. When the modulus of elasticity increases with time, $f_{ij} > 0$. If the modulus of elasticity decreases with time, $-1 < f_{ij} < 0$.

The stress-strain-time relationship for the *i*-th unit of the model in Fig. 3 for the *j*-th layer of the beam under constant applied stress, σ_j, is obtained by using the equations for equilibrium

$$\sigma_{D_{ij}} + \sigma_{E_{ij}} = \sigma_j, \qquad \sigma_{D_{ij}} + \sigma_{H_{ij}} = \sigma_j \tag{4}$$

where $\sigma_{D_{ij}}$, $\sigma_{H_{ij}}$ and $\sigma_{E_{ij}}$ are the stresses in dashpots with coefficients of viscosities, $\eta_{D_{ij}}$ and $\eta_{H_{ij}}$, and in the spring, respectively.

The stresses involved in (4) are expressed by applying the Hooke's law

$$\sigma_{D_{ij}} = \eta_{D_{ij}}\dot{\varepsilon}_{i}, \qquad \sigma_{H_{ij}} = \eta_{H_{ij}}\dot{\varepsilon}_{H_i}, \qquad \sigma_{E_{ij}} = E_{ij} \rightleftarrows \varepsilon_{E_i} \tag{5}$$

where ε_{H_i} and ε_{E_i} are the strains in the dashpot with coefficient of viscosity, $\eta_{H_{ij}}$, and in the spring, respectively. The strains are connected as

$$\varepsilon_{H_i} + \varepsilon_{E_i} = \varepsilon_i \tag{6}$$

By using of (4), (5) and (6), one obtains the following equation

$$\ddot{\varepsilon}_i + E_{ij}\alpha_{ij}\dot{\varepsilon}_i = E_{i}\,\beta_{ij}\sigma_j \tag{7}$$

where

$$\alpha_{ij} = \frac{\eta_{H_{ij}} + \eta_{D_{ij}}}{\eta_{D_{ij}}\eta_{H_{ij}}} \tag{8}$$

$$\beta_{ij} = \frac{1}{\eta_{D_{ij}}\eta_{H_{ij}}} \tag{9}$$

The solution of (7) is found as

$$\begin{aligned}\varepsilon_i = {} & \sigma_j \frac{\beta_{ij}}{\alpha_{ij}} t + \sigma_j \frac{\beta_{ij}}{\alpha_{ij}} \frac{e^{-\alpha_{ij}\theta_{ij}t}}{\alpha_{ij}\theta_{ij}} \left\{ 1 + \frac{\delta_{ij}}{\alpha_{ij}\theta_{ij}} \left(\alpha_{ij}\theta_{ij}t + 1\right) \right. \\ & \left. + \frac{\delta_{ij}\left(\delta_{ij} - 1\right)}{2} \left[t^2 + \frac{2}{\left(\alpha_{ij}\theta_{ij}\right)^2} \left(\alpha_{ij}\theta_{ij}t + 1\right) \right] \right\} \\ & - \sigma_j \frac{\beta_{ij}}{\alpha_{ij}^2\theta_{ij}} \left[1 + \frac{\delta_{ij}}{\alpha_{ij}\theta_{ij}} + \frac{\delta_{ij}\left(\delta_{ij} - 1\right)}{\left(\alpha_{ij}\theta_{ij}\right)^2} \right]\end{aligned} \tag{10}$$

where

$$\theta_{ij} = E_{0_{ij}}\left(1 + f_{ij}\right) \tag{11}$$

$$\delta_{ij} = \alpha_{ij} E_{0_{ij}} f_{ij} \tag{12}$$

The stress-strain-time relationship is found by summation of the strains in the units of the model. The result is

$$\begin{aligned}\varepsilon_{\vec{\tau}} = \sum_{i=1}^{i=n} {} & \left\{ \sigma_j \frac{\beta_{ij}}{\alpha_{ij}} t + \sigma_j \frac{\beta_{ij}}{\alpha_{ij}} \frac{e^{-\alpha_{ij}\theta_{ij}t}}{\alpha_{ij}\theta_{ij}} \left\{ 1 + \frac{\delta_{ij}}{\alpha_{ij}\theta_{ij}} \left(\alpha_{ij}\theta_{ij}t + 1\right) \right. \right. \\ & \left. + \frac{\delta_{ij}\left(\delta_{ij} - 1\right)}{2} \left[t^2 + \frac{2}{\left(\alpha_{ij}\theta_{ij}\right)^2} \left(\alpha_{ij}\theta_{ij}t + 1\right) \right] \right\} \\ & \left. - \sigma_j \frac{\beta_{ij}}{\alpha_{ij}^2\theta_{ij}} \left[1 + \frac{\delta_{ij}}{\alpha_{ij}\theta_{ij}} + \frac{\delta_{ij}\left(\delta_{ij} - 1\right)}{\left(\alpha_{ij}\theta_{ij}\right)^2} \right] \right\}\end{aligned} \tag{13}$$

Each layer of the beam exhibits continuous material inhomogeneity in width, thickness and length directions. Therefore, material properties vary continuously in the volume of the layer.

The distributions of the modulus of elasticity and the coefficients of viscosity for the *i*-th unit of the model in the cross-section of *j*-th layer are described by using the following exponential functions (it should be noted that exponential functions are frequently applied for treating the distribution of material properties in continuously inhomogeneous (functionally graded) structural members (Kurşun *et al*. 2012, 2014))

$$E_{ij}^{'} = E_{ij} e^{\lambda_{ij}\vec{\tau}\frac{\frac{b}{2}+y_3}{b} + \mu_{ij}\frac{z_3 - z_{3j}}{z_{3j+1} - z_{3j}}} \tag{14}$$

$$\eta_{D_{ij}} = \eta_{D_{Rij}} e^{\phi_{ij}\frac{\frac{b}{2}+y_3}{b}+\psi_{ij}\frac{z_3-z_{3j}}{z_{3j+1}-z_{3j}}} \tag{15}$$

$$\eta_{H_{ij}} = \eta_{H_{Rij}} e^{\omega_{ij}\frac{\frac{b}{2}+y_3}{b}+\rho_{ij}\frac{z_3-z_{3j}}{z_{3j+1}-z_{3j}}} \tag{16}$$

where

$$i = 1,2,\dots n \tag{17}$$

$$j = 1,2,\dots m \tag{18}$$

$$-\frac{b}{2} \le y_3 \le \frac{b}{2} \tag{19}$$

$$z_{3j} \le z_3 \le z_{3j+1} \tag{20}$$

In formulae (14)–(20), E_{ij}, $\eta_{D_{Rij}}$ and $\eta_{H_{Rij}}$ are the values of $E_{ij}^{'}$, $\eta_{D_{ij}}$ and $\eta_{H_{ij}}$ in the upper left-hand vertex of cross-section of the *j*-th layer, respectively. The distributions of $E_{ij}^{'}$, $\eta_{D_{ij}}$ and $\eta_{H_{ij}}$ along the beam width are controlled by the parameters, λ_{ij}, ϕ_{ij} and ω_{ij}, respectively. The parameters, μ_{ij}, ψ_{ij} and ρ_{ij}, control the distributions of $E_{ij}^{'}$, $\eta_{D_{ij}}$ and $\eta_{H_{ij}}$ along the thickness of the layer, respectively. In fact, λ_{ij}, ϕ_{ij}, ω_{ij}, μ_{ij}, ψ_{ij} and ρ_{ij} dictate the modulus of elasticity and the coefficients of viscosity variation profiles in the cross-section of the layer. The coordinates of the upper and lower surfaces of the layer are denoted by z_{3j} and z_{3j+1}, respectively (Fig. 2).

The distributions of $E_{0_{ij}}$, $\eta_{D_{Rij}}$ and $\eta_{H_{Rij}}$ along the beam length are written as

$$E_{0_{ij}} = E_{0L_{ij}} e^{g_{ij}\frac{x_3}{l_1+l_2}} \tag{21}$$

$$\eta_{D_{Rij}} = \eta_{DL_{Rij}} e^{s_{ij}\frac{x_3}{l_1+l_2}} \tag{22}$$

$$\eta_{H_{Rij}} = \eta_{HL_{Rij}} e^{r_{ij}\frac{x_3}{l_1+l_2}} \tag{23}$$

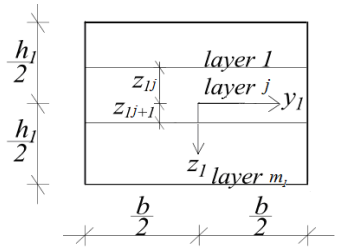

Fig. 4 Cross-section of the lower delamination crack arm

where

$$i = 1,2,\dots n \tag{24}$$

$$j = 1,2,\dots m \tag{25}$$

$$0 \le x_3 \le l_1 + l_2 \tag{26}$$

In formulae (21)–(26), x_3 is the longitudinal centroidal axis of the beam (Fig. 1), $E_{0L_{ij}}$, $\eta_{DL_{Rij}}$ and $\eta_{HL_{Rij}}$ are the values of $E_{0_{ij}}$, $\eta_{D_{Rij}}$ and $\eta_{H_{Rij}}$ at the left-hand end of the beam, respectively. The parameters, g_{ij}, s_{ij} and r_{ij}, control the distributions of $E_{0_{ij}}$, $\eta_{D_{Rij}}$ and $\eta_{H_{Rij}}$ along the length of the beam, respectively.

Since the material exhibits creep behavior, the strain energy release rate for the delamination crack in the beam under consideration is a function of time. In the present paper, a time-dependent solution to the strain energy release rate, G, that takes into account the creep and the change of the modulus of elasticity with time is derived by applying the formula (Rizov 2020)

$$G = \frac{1}{b}\left(\overrightarrow{\leftarrow} \sum_{j=1}^{j=m_1} \iint_{(A_j)} u_{0j} dA - \overrightarrow{\leftarrow} \sum_{j=1}^{j=m} \iint_{(A_j)} u_{0uj} dA \right) \tag{27}$$

where m_1 is the number of layers in the lower crack arm (Fig. 4), u_{0j} is the time-dependent strain energy density in the *j*-th layer behind the crack tip, A_j is the area of the cross-section of the layer, u_{0uj} is the time-dependent strain energy density in the *j*-th layer of the beam portion, B_2B_3, ahead of the crack tip. It should be mentioned that formula (27) takes into account the fact that the strain energy in the upper crack arm is zero since this crack arm is free of stresses.

The time-dependent strain energy density in the *j*-th layer of the lower crack arm is written as

$$u_{0j} = \frac{1}{2}\sigma_j \varepsilon_{\overrightarrow{\leftarrow}} \tag{28}$$

where $\varepsilon_{\overrightarrow{\leftarrow}}$ is a function of time (refer to Eq. (13)).

In the present paper, the distribution of strains in the beam is treated by applying the Bernoulli's hypothesis for plane sections since the beam under consideration has high length to thickness ratio. Therefore, the distribution of strains in the cross-section of the lower crack arm is written as

$$\varepsilon = \varepsilon_{C_1} + \kappa_{y_1 \overrightarrow{\leftarrow}} y_1 + \kappa_{z_1} z_1 \tag{29}$$

where y_1 and z_1 are the centroidal axes of the lower crack arm cross-section, ε_{C_1} is the strain in the centre of the cross-section. The curvatures in the planes, x_1y_1 and x_1z_1, are denoted by κ_{y_1} and κ_{z_1}, respectively.

The strain in the centre and the two curvatures are determined by using the following equations for equilibrium of elementary forces in the cross-section of the lower crack arm

$$N_1 = \sum_{j=1}^{j=m_1} \iint_{(A_j)} \sigma_j dy_1 dz_1 \tag{30}$$

$$M_{y_1} = \sum_{j=1}^{j=m_1} \iint_{(A_j)} \sigma_j z_1 dy_1 dz_1 \tag{31}$$

$$M_{z_1} = \sum_{j=1}^{j=m_1} \iint_{(A_j)} \sigma_j y_1 dy_1 dz_1 \tag{32}$$

where the axial force, N_1, and the bending moments M_{y_1} and M_{z_1} with respect to y_1 and z_1 are written as (Fig. 1)

$$N_1 = 0 \tag{33}$$

$$M_{y_1} = Fl_2 \tag{34}$$

$$M_{z_1} = 0 \tag{35}$$

The stress, σ_j, is expressed as a function of t, y_1 and z_1 by using dependences (13) and (29). The result is

$$\sigma_j = \left(\varepsilon_{C_1} + \kappa_{y_1} y_1 + \kappa_{z_1} z_1\right)\left\{\sum_{i=1}^{i=n}\left\{\frac{\beta_{ij}}{\alpha_{ij}}t + \frac{\beta_{ij}}{\alpha_{ij}}\frac{e^{-\alpha_{ij}\theta_{ij}t}}{\alpha_{ij}\theta_{ij}}\left\{1 + \frac{\delta_{ij}}{\alpha_{ij}\theta_{ij}}\left(\alpha_{ij}\theta_{ij}t + 1\right)\right.\right.\right.$$
$$\left.\left.\left. + \frac{\delta_{ij}\left(\delta_{ij}-1\right)}{2}\left[t^2 + \frac{2}{\left(\alpha_{ij}\theta_{ij}\right)^2}\left(\alpha_{ij}\theta_{ij}t + 1\right)\right]\right\} - \frac{\beta_{ij}}{\alpha_{ij}^2\theta_{ij}}\left[1 + \frac{\delta_{ij}}{\alpha_{ij}\theta_{ij}} + \frac{\delta_{ij}\left(\delta_{ij}-1\right)}{\left(\alpha_{ij}\theta_{ij}\right)^2}\right]\right\}\right\}^{-1} \tag{36}$$

After substituting of (36) in (30), (31) and (32), the three equations for equilibrium are solved with respect to the strain in the centre and the two curvatures at various values of time by using the MatLab computer program.

The time-dependent strain energy density in the *j*-th layer of the beam portion, B_2B_3, is found as

$$u_{0uj} = \frac{1}{2}\sigma_{uj}\varepsilon_{u} \tag{37}$$

where the strain, ε_u, is obtained, respectively, by replacing of ε_{C_1}, κ_{y_1}, κ_{z_1}, y_1 and z_1 with ε_{C_2}, κ_{y_2}, κ_{z_2}, y_2 and z_2 in (29).

Here, ε_{C_2}, κ_{y_2} and κ_{z_2} are the strain in the centre of the cross-section of portion, B_2B_3, of the beam, the curvatures in planes, x_2y_2 and x_2z_2, respectively. The centroidal axes of the beam are denoted by y_2 and z_2. The quantities, ε_{C_2}, κ_{y_2} and κ_{z_2}, are determined by using the equations for equilibrium (30), (31) and (32). For this purpose, m_1, σ_j, y_1 and z_1 are replaced

with m, σ_{uj}, y_2 and z_2, respectively. The stress, σ_{uj}, is obtained by replacing of ε_{C_1}, κ_{y_1}, κ_{z_1}, y_1 and z_1 with ε_{C_2}, κ_{y_2}, κ_{z_2}, y_2 and z_2 in formula (36).

After substituting of the strain energy densities in (27), the strain energy release rate is obtained at various values of the time. The integration in (27) is carried-out by using the MatLab computer program.

The *J*-integral approach is also used to analyze the delamination in Fig. 1 (Broek 1986). The *J*-integral is solved along the integration contour, K, shown by a dashed line in Fig. 1. The *J*-integral value in the upper delamination crack arm is zero since this crack arm is free of stresses. Therefore, the time-dependent solution of the *J*-integral is written as

$$J_{\rightleftarrows} = J_{K_1} + J_{K_2} \tag{38}$$

where J_{K_1} and J_{K_2} are the *J*-integral values in segments, K_1 and K_2, of the integration contour, respectively. Segments, K_1 and K_2, coincide with the cross-sections of the lower crack arm and the un-cracked beam portions, respectively (Fig. 1).

The *J*-integral in segment, K_1, of the integration contour is written as

$$J_{K_1} = \sum_{j=1}^{j=m_1} \int_{z_{1j}}^{z_{1j+1}} \left[u_{0j} \cos \alpha_{K_1} - \left(p_{xj} \frac{\partial u}{\partial x} + p_{yj} \frac{\partial v}{\partial x} \right) \right] ds \tag{39}$$

where α_{K_1} is the angle between the outwards normal vector to the contour of integration and the crack direction, u and v are the horizontal and vertical components of displacement vector, p_{xj} and p_{yj} are the horizontal and vertical components of stress vector, ds is a differential element along the contour of integration.

The components of (39) are obtained as

$$\cos \alpha_{K_1} = -1 \tag{40}$$

$$p_{xj} = -\sigma_j \tag{41}$$

$$p_{yj} = 0 \tag{42}$$

$$ds = dz_1 \tag{43}$$

$$\frac{\partial u}{\partial x} = \varepsilon \tag{44}$$

The *J*-integral in segment, K_2, is expressed as

$$J_{K_2} = \sum_{j=1}^{j=m_{\rightleftarrows}} \int_{z_{2j}}^{z_{2j+1}} \left[u_{0uj} \cos \alpha_{K_2} - \left(p_{xuj} \frac{\partial u}{\partial x_{K_2}} + p_{yuj} \frac{\partial v}{\partial x_{K_2}} \right) \right] ds_{K_2} \tag{45}$$

where

$$cos\,\alpha_{K_2} = 1 \tag{46}$$

$$p_{xuj} = \sigma_{uj} \tag{47}$$

$$p_{yuj} = 0 \tag{48}$$

$$ds_{K_2} = -dz_2 \tag{49}$$

$$\frac{\partial u}{\partial x_{K_2}} = \varepsilon_u \tag{50}$$

The average value of the *J*-integral along the delamination crack front is written as

$$J_{av} = \frac{1}{b}\int_{-\frac{b}{2}}^{\frac{b}{2}} J dy_1 \tag{51}$$

By combining of (38), (39) and (51), one derives

$$\begin{aligned} J_{av} = \frac{1}{b}\Bigg\{ & \int_{-\frac{b}{2}}^{\frac{b}{2}} \sum_{j=1}^{j=m_1} \int_{z_{1j}}^{z_{1j+1}} \left[u_{0j}\, cos\,\alpha_{K_1} - \left(p_{xj}\frac{\partial u}{\partial x} + p_{yj}\frac{\partial v}{\partial x} \right) \right] ds dy_1 \\ & + \int_{-\frac{b}{2}}^{\frac{b}{2}} \sum_{j=1}^{j=m_{\rightleftarrows}} \int_{z_{2j}}^{z_{2j+1}} \left[u_{0uj}\, cos\,\alpha_{K_2} - \left(p_{xuj}\frac{\partial u}{\partial x_{K_2}} + p_{yuj}\frac{\partial v}{\partial x_{K_2}} \right) \right] ds_{K_2} dy_1 \Bigg\} \end{aligned} \tag{52}$$

The solution (52) is used to obtain the *J*-integral at various values of time. The integration in (52) is carried-out by the MatLab computer program. It should be noted that the *J*-integral values obtained by applying (52) are exact matches of the strain energy release rates calculated by using (27). This fact proves the correctness of delamination analysis developed in the present paper. The accuracy of the analysis of the strain energy release rate is confirmed likewise analytically. For this purpose, the fact that the *J*-integral solution (52) matches the solution of the strain energy release rate (27) is proved also in the following way. By using (28) and (40)–(44), one derives

$$u_{0j}\, cos\,\alpha_{K_1} - \left(p_{xj}\frac{\partial u}{\partial x} + p_{yj}\frac{\partial v}{\partial x} \right) = u_{0j}. \tag{53}$$

Analogically, by using (37) and (46)–(50), one obtains

$$u_{0uj}\, cos\,\alpha_{K_2} - \left(p_{xuj}\frac{\partial u}{\partial x_{K_2}} + p_{yuj}\frac{\partial v}{\partial x_{K_2}} \right) = -u_{0uj}. \tag{54}$$

By substituting of (53) and (54) in (52), and by taking into account the fact that the integrals in (52) can be replaced by double integrals in the cross-section of the *j*-th layer of the beam, formula (52) is re-written as

$$J_{av} = \frac{1}{b}\left(\rightleftarrows \sum_{j=1}^{j=m_1} \iint_{(A_j)} u_{0j} dA - \rightleftarrows \sum_{j=1}^{j=m} \iint_{(A_j)} u_{0uj} dA \right). \tag{55}$$

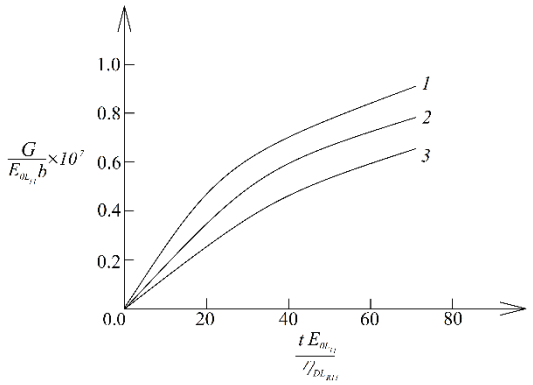

Fig. 5 The strain energy release rate in non-dimensional form, $G_N = G/\left(E_{0L_{11}}b\right)$, presented as a function of the non-dimensional time, $t_N = tE_{0L_{11}}/\eta_{DL_{R11}}$ (curve 1 - at $f_{11} = -0.4$, curve 2 – at $f_{11} = 0.4$ and curve 3 – at $f_{11} = 0.8$)

which is exact match of the solution of the strain energy release rate (27).

3. Parametric analysis

A parametric analysis is carried-out of the delamination in the multilayered beam in Fig. 1. For this purpose, calculations of the strain energy release rate are performed by applying the time-dependent solution (27). The strain energy release rate is expressed in non-dimensional form by applying the formula $G_N = G/\left(E_{0L_{11}}b\right)$. A viscoelastic model with four units is used. A beam configuration with three layers is considered in the parametric analysis. The thickness of each layer is h_t. There are two layers in the lower crack arm. Thus, the thicknesses of the lower and upper crack arms are $h_1 = 2h_t$ and $h_2 = h_t$, respectively. It is assumed that $b = 0.015$ m, $h_t = 0.006$ m, $l_1 = 0.200$ m, $l_2 = 0.050$ m and $F = 5$ Nm.

The variation of the strain energy release rate with time and the influence of the change of the modulus of elasticity with time are analyzed. For this purpose, the strain energy release rate is obtained at various values of time for three values of f_{11}. The strain energy release rate in non-dimensional form is presented as a function of non-dimensional time in Fig. 5 at three values of f_{11}. The time is expressed in non-dimensional form by using the formula $t_N = tE_{0L_{11}}/\eta_{DL_{R11}}$.

It is evident from Fig. 5 that the strain energy release rate increases with time which is due to the creep. One can observe also in Fig. 5 that increase of f_{11} leads to decrease of the strain energy release rate (this finding indicates that the strain energy release rate decreases with increasing of the modulus of elasticity with time).

The influence of the material inhomogeneity on the strain energy release rate is also analyzed. First, the effect of the variation of the modulus of elasticity in the cross-section of the layer 1 is evaluated by carrying-out calculations at various values of λ_{11} and μ_{11}. The results obtained are illustrated in Fig. 6 where the strain energy release rate in non-dimensional form is presented as a function of λ_{11} at three values of μ_{11}. The curves in Fig. 6 indicate that the strain energy release rate decreases with increasing of λ_{11}. It can be observed also in Fig. 6 that the increase of μ_{11} leads to decrease of the strain energy release rate.

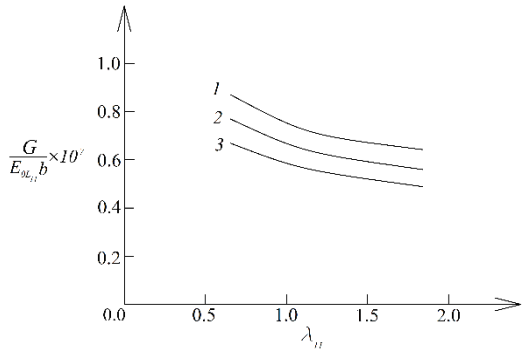

Fig. 6 The strain energy release rate in non-dimensional form, $G_N = G/\left(E_{0L_{11}}b\right)$, presented as a function of parameter, λ_{11}, controlling the distribution of $E_{ij}^{'}$ in layer 1 along the beam width (curve 1 – at $\mu_{11} = 0.5$, curve 2 – at $\mu_{11} = 1.0$ and curve 3 – at $\mu_{11} = 2.0$)

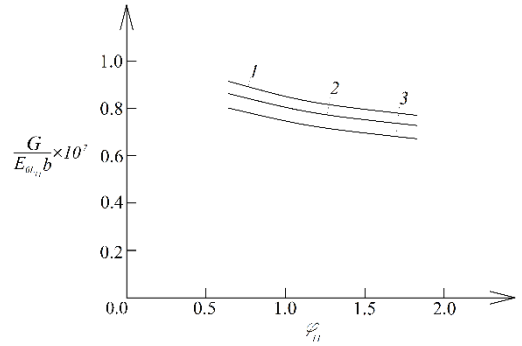

Fig. 7 The strain energy release rate in non-dimensional form, $G_N = G/\left(E_{0L_{11}}b\right)$, presented as a function of parameter, ϕ_{11}, controlling the distribution of $\eta_{D_{ij}}$ in layer 1 along the beam width (curve 1 – at $\psi_{11} = 0.5$, curve 2 – at $\psi_{11} = 1.0$ and curve 3 – at $\psi_{11} = 2.0$)

The effect of the continuous variation of the coefficient of viscosity, $\eta_{D_{11}}$, in the cross-section of layer 1 is indicated in Fig. 7 by presenting of the strain energy release rate as a function of ϕ_{11} at three values of ψ_{11}. One can observe in Fig. 7 that the strain energy release rate decreases with increasing of ϕ_{11}. The increase of material property, ψ_{11}, leads also to decrease of the strain energy release rate (Fig. 7).

Calculations of the strain energy release rate are performed at various values of ω_{11} and ρ_{11} in order to assess the influence of the continuous change of the coefficient of viscosity, $\eta_{H_{11}}$, in the cross-section of layer 1 of the beam. The strain energy release rate in non-dimensional from is presented as a function of ω_{11} in Fig. 8 at three values of ρ_{11}. The curves in Fig. 8 show that the strain energy release rate decreases with increasing of ω_{11} and ρ_{11}.

One can get an idea about the influence of the continuous variation of the coefficients of viscosity, $\eta_{D_{11}}$ and $\eta_{H_{11}}$, along the length of the beam on the strain energy release rate from Fig. 9 where the strain energy release rate in non-dimensional form is presented as a function of s_{11} at three values of r_{11}. It is evident that the strain energy release rate decreases with increasing of s_{11} and r_{11} (Fig. 9).

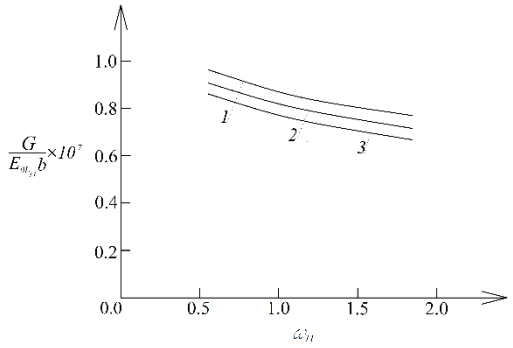

Fig. 8 The strain energy release rate in non-dimensional from, $G_N = G/\left(E_{0L_{11}}b\right)$, presented as a function of parameter, ω_{11}, controlling the distribution of $\eta_{H_{ij}}$ in layer 1 along the beam width (curve 1 – at $\rho_{11} = 0.5$, curve 2 – at $\rho_{11} = 1.0$ and curve 3 – at $\rho_{11} = 2.0$)

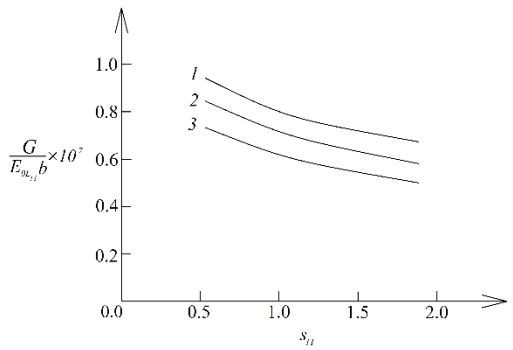

Fig. 9 The strain energy release rate in non-dimensional form, $G_N = G/\left(E_{0L_{11}}b\right)$, presented as a function of parameter, s_{11}, controlling the distribution of $\eta_{D_{Rij}}$ in layer 1 along the beam length (curve 1 – at $r_{11} = 0.5$, curve 2 – at $r_{11} = 1.0$ and curve 3 – at $r_{11} = 2.0$)

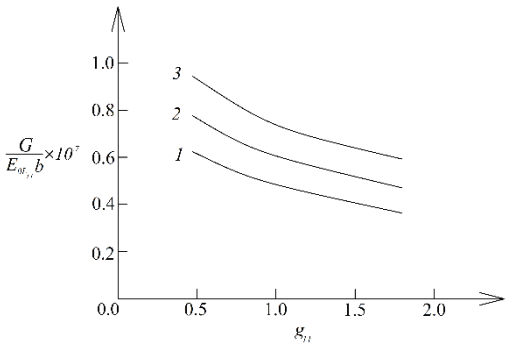

Fig. 10 The strain energy release rate in non-dimensional form, $G_N = G/\left(E_{0L_{11}}b\right)$, presented as a function of parameter, g_{11}, controlling the distribution of $E_{0_{ij}}$ in layer 1 along the beam length (curve 1 – for viscoelastic model with two units, curve 2 – for viscoelastic model with three units and curve 3 - for viscoelastic model with four units)

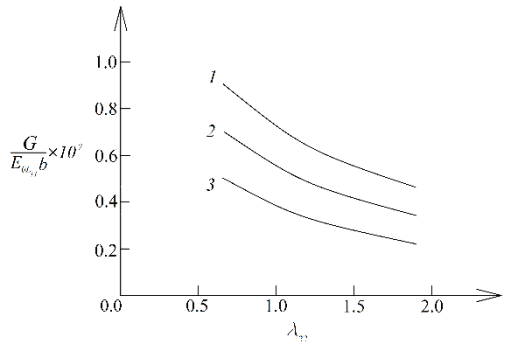

Fig. 11 The strain energy release rate in non-dimensional form, $G_N = G/\left(E_{0L_{11}}b\right)$, presented as a function of parameter, λ_{22}, controlling the distribution of $E_{22}^{'}$ ⇄ in layer 2 along the beam width (curve 1 – for beam configuration with three layers, curve 2 – for beam configuration with four layers and curve 3 – for beam configuration with five layers)

The influence of the number of the units in the viscoelastic model is investigated too. For this purpose, calculations of the strain energy release rate are performed by using models with two and three units in the model.

The results obtained are shown in Fig. 10 where the strain energy release rate in non-dimensional form is presented as a function of g_{11} (the material property, g_{11}, controls the continuous variation of the modulus of elasticity in layer 1 along the beam length) for models with two, three and four units.

It can be observed in Fig. 10 that the strain energy release rate decreases with increasing of g_{11}. Concerning the influence of the number of units in the viscoelastic model, the curves in Fig. 10 indicate that the strain energy release rate increases with increasing the number of units (this finding is attributed to the increase of the strain with increasing the number of the units in the viscoelastic model at a constant applied stress).

The effect of the number of layers on the strain energy release rate is also analyzed. Beam configurations with three, four and five layers are considered. The thickness of each layer is h_t. The stain energy release rate is presented as a function of λ_{22} in Fig. 11 for the considered beam configurations. One can observe in Fig. 11 that increase of the number of layers causes decrease of the strain energy release rate.

4. Conclusions

A delamination in a multilayered inhomogeneous beam structure exhibiting linear creep behaviour is analyzed. The creep is treated by using a viscoelastic model consisting of an arbitrary number of consecutively connected units. Each unit has one spring and two dashpots. The modulus of elasticity of the spring in each unit of the model changes with time. Each layer of the beam is continuously inhomogeneous in width, thickness and length directions. Therefore, the coefficients of viscosity and the modulii of elasticity change continuously along the width, thickness and length in each layer.

A time-dependent solution to the strain energy release rate that accounts for the creep and for the change of the modulii of elasticity with time is derived by considering the time-dependent

strain energy. The delamination is analyzed also by applying the *J*-integral for verification. A parametric analysis of the strain energy release rate is carried-out. The analysis reveals that the strain energy release rate increases with time due to the creep. It is found that the increase of the modulii of elasticity with time leads to decrease of the strain energy release rate. Concerning the effect of material inhomogeneity, the investigation indicates that the strain energy release rate decreases with increasing of λ_{11}, μ_{11}, ϕ_{11}, ψ_{11}, ω_{11}, ρ_{11}, s_{11}, r_{11} and g_{11}. The increase of the number of units in the viscoelastic model leads to increase of the strain energy release rate (this behavior is due to increase of the strain with increase of the number of units in the model under a constant applied stress). The effect of the number of layers in the beam structure is also studied. It is found that increase of the number of layers causes decrease of the strain energy release rate. It should be mentioned that the solution derived in the present paper can be extended for analyzing of the strain energy release rates for multiple delaminations in the layered structure under creep. For this purpose, the time-dependent strain energy in the beam has to be expressed as a function of the lengths of the delaminations. Then the strain energy release rates can be obtained by differentiating of the time-dependent strain energy with respect to the areas of the delaminations.

References

Abderezak, R., Daouadji, T.H. and Rabia, B. (2021), "Aluminum beam reinforced by externally bonded composite materials", *Adv. Mater. Res., Int. J.*, **10**(1), 23-44. http://doi.org/10.12989/amr.2021.10.1.023

Ahmed, R.A., Fenjan, R.A., Hamad, L.B. and Faleh, N.M. (2020), "A review of effects of partial dynamic loading on dynamic response of nonlocal functionally graded material beams", *Adv. Mater. Res., Int. J.*, **9**(1), 33-48. http://doi.org/10.12989/amr.2020.9.1.033

Arda, M. (2020), "Axial dynamics of functionally graded Rayleigh-Bishop nanorods", *Microsyst. Technol.*, **1**, 1-17. https://doi.org/10.1007/s00542-020-04950-2

Arda, M. and Aydogdu, M. (2016), "Torsional wave propagation of CNTS via different nonlocal gradient theories", *Proceedings of the 23rd International Congress on Sound and Vibration 8ICSV23*, Athens, Greece, July. https://doi.org/10.1007/s00339-016-9751-1

Aydogdu, M., Arda, M. and Filiz, S. (2018), "Vibration of axially functionally graded nano rods and beams with a variable nonlocal parameter", *Adv. Nano Res., Int. J.*, **6**(3), 257-278. https://doi.org/10.12989/anr.2018.6.3.257

Broek, D. (1986), *Elementary Engineering Fracture Mechanics*, Springer.

Butcher, R.J., Rousseau, C.E. and Tippur, H.V. (1999), "A functionally graded particulate composite: Measurements and Failure Analysis", *Acta. Mater.*, **47**(2), 259-268. https://doi.org/10.1016/S1359-6454(98)00305-X

Gasik, M.M. (2010), "Functionally graded materials: bulk processing techniques", *Int. J. Mater. Product Technol.*, **39**(1-2), 20-29. https://doi.org/10.1504/IJMPT.2010.034257

Hedia, H.S., Aldousari, S.M., Abdellatif, A.K. and Fouda, N.A. (2014), "New design of cemented stem using functionally graded materials (FGM)", *Biomed. Mater. Eng.*, **24**(3), 1575-1588. https://doi.org/10.3233/BME-140962

Hsueh, C.H., Tuan, W.H. and Wei, W.C.J. (2009), "Analyses of steady-state interface fracture of elastic multilayered beams under four-point bending", *Scripta Mater.*, **60**, 721-724. https://doi.org/10.1016/j.scriptamat.2009.01.001

Hutchinson, J. and Suo, Z. (1991), "Mixed mode cracking in layered materials", *Adv. Appl. Mech.*, **29**, 63-191. https://doi.org/10.1016/S0065-2156(08)70164-9

Kurşun, A. and Topçu, M. (2013), "Thermal stress analysis of functionally graded disc with variable thickness due to linearly increasing temperature load", *Arab J. Sci. Eng.*, **38**, 3531-3549.

https://doi.org/10.1007/s13369-013-0626-x
Kurşun, A., Topçu, M. and Yücel, U. (2012), "Stress analysis of a rotating fgm circular disc with exponentially-varying properties", *Proceedings of the ASME 2012 International Mechanical Engineering Congress & Exposition IMECE2012*, Houston, TX, USA, November, pp. 1-5. https://doi.org/10.1115/IMECE2012-85592
Kurşun, A., Kara, E., Çetin, E., Aksoy, Ş. and Kesimli, A. (2014), "Mechanical and thermal stresses in functionally graded cylinders", *Int. J. Mech. Aerosp. Indust. Mechatron. Manuf. Eng.*, **8**(2), 303-308. https://doi.org/10.5281/zenodo.1090725
Mahamood, R.M. and Akinlabi, E.T. (2017), *Functionally Graded Materials*, Springer.
Malzbender, J. (2004), "Mechanical and thermal stresses in multilayered materials", *J. Appl. Phys.*, **95**(4), 1780. https://doi.org/10.1063/1.1642289
Markworth, A.J., Ramesh, K.S. and Parks, Jr.W.P. (1995), "Review: modeling studies applied to functionally graded materials", *J. Mater. Sci.*, **30**(3), 2183-2193. https://doi.org/10.1007/BF01184560
Miyamoto, Y., Kaysser, W.A., Rabin, B.H., Kawasaki, A. and Ford, R.G. (1999), *Functionally Graded Materials*: *Design*, *Processing and Applications*, Kluwer Academic Publishers, Dordrecht/London/Boston.
Nemat-Allal, M.M., Ata, M.H., Bayoumi, M.R. and Khair-Eldeen, W. (2011), "Powder metallurgical fabrication and microstructural investigations of Aluminum/Steel functionally graded material", *Mater. Sci. Applicat.*, **2**(5), 1708-1718. https://doi.org/10.4236/msa.2011.212228.
Nguyen, S.N., Lee, J. and Cho, M. (2015), "Efficient higher-order zig-zag theory for viscoelastic laminated composite plates", *Int. J. Solids Struct.*, **62**, 174-185. https://doi.org/10.1016/j.ijsolstr.2015.02.027
Nguyen, S.N., Lee, J., Han, J.W. and Cho, M. (2020), "A coupled hygrothermo-mechanical viscoelastic analysis of multilayered composite plates for long-term creep behaviors", *Compos. Struct.*, **242**, 112030. https://doi.org/10.1016/j.compstruct.2020.112030
Rabia, B., Daouadji, T.H. and Abderezak, R. (2020), "Predictions of the maximum plate end stresses of imperfect FRP strengthened RC beams: study and analysis", *Adv. Mater. Res., Int. J.*, **9**(4), 265-287. https://doi.org/10.12989/amr.2020.9.4.265
Rizov, V.I. (2016), "Elastic-plastic fracture of functionally graded circular shafts in torsion", *Adv. Mater. Res., Int. J.*, **5**(4), 299-318. https://doi.org/10.12989/amr.2016.5.4.299
Rizov, V.I. (2017), "Analysis of longitudinal cracked two-dimensional functionally graded beams exhibiting material non-linearity", *Frattura ed Integrità Strutturale*, **41**, 498-510. https://doi.org/10.3221/IGF-ESIS.41.61
Rizov, V.I. (2018), "Analysis of cylindrical delamination cracks in multilayered functionally graded non-linear elastic circular shafts under combined loads", *Frattura ed Integrità Strutturale*, **46**, 158-217. https://doi.org/10.3221/IGF-ESIS.46.16
Rizov, V.I. (2020), "Longitudinal fracture analysis of inhomogeneous beams with continuously changing radius of cross-section along the beam length", *Strength Fract. Complex.: Int. J.*, **13**, 31-43. https://doi.org/10.3233/SFC-200250
Rizov, V.I. (2021), "Viscoelastic inhomogeneous beams under step loading: a longitudinal fracture analysis", *IOP Conference Series: Mater. Sci. Eng.*, **1031**, 012008. https://doi.org/10.1088/1757-899X/1031/1/01200
Rizov, V. and Altenbach, H. (2019), "Application of the Classical Beam Theory for Studying Lengthwise Fracture of Functionally Graded Beams", *TECHNISCHE MECHANIK*, **39**(2), 229-240. https://doi.org/10.24352/UB.OVGU-2019-021
Rizov, V. and Altenbach, H. (2020a), "Longitudinal fracture analysis of inhomogeneous beams with continuously varying sizes of the cross-section along the beam length", *Frattura ed Integrità Strutturale*, **53**, 38-50. https://doi.org/10.3221/IGF-ESIS.53.04
Rizov, V.I. and Altenbach, H. (2020b), "Influence of material non-linearity on delamination in multilayered three-point bending beams", *J. Theor. Appl. Mech.*, **50**, 70-82. https://doi.org/10.7546/JTAM.50.20.01.07
Uymaz, B. (2013), "Forced vibration analysis of functionally graded beams using nonlocal elasticity", *Compos. Struct.*, **105**, 227-239. https://doi.org/10.1016/j.compstruct.2013.05.006
Uymaz, B. (2014a), "Corrigendum to "Forced vibration analysis of functionally graded beams using

nonlocal elasticity", *Compos*. *Struct*., **107**, 749-461. https://doi.org/10.1016/j.compstruct.2013.09.038
Uymaz, B. (2014b), "Comparison of free vibration and buckling behavior of cross-ply laminated plates with isotropic and orthotropic plates", *Int*. *J*. *Eng*. *Appl*. *Sci*., **5**(4), 13-34. https://dergipark.org.tr/tr/pub/ijeas/issue/23589/251204
Wu, X.L., Jiang, P., Chen, L., Zhang, J.F., Yuan, F.P. and Zhu, Y.T. (2014), "Synergetic strengthening by gradient structure", *Mater*. *Res*. *Lett*., **2**(1), 185-191. https://doi.org/10.1080/21663831.2014.935821

CC